Spectral response of point-contact Josephson junctions

Tolner, H.

Published in:
Journal of Applied Physics

DOI:
10.1063/1.323658

Publication date:
1977

Spectral response of point-contact Josephson junctions

H. Tolner

Citation: Journal of Applied Physics **48**, 691 (1977); doi: 10.1063/1.323658
View online: https://doi.org/10.1063/1.323658
View Table of Contents: http://aip.scitation.org/toc/jap/48/2
Published by the American Institute of Physics

Spectral response of point-contact Josephson junctions

H. Tolner

Kapteyn Astronomical Institute, Department of Space Research, University of Groningen, Groningen, The Netherlands
(Received 30 August 1976)

The spectral response of niobium point-contact Josephson junctions with resistance values R between 1 kΩ and 10 Ω has been measured. For $R \gtrsim 100$ Ω the response peaks at maxima of $d^2\bar{V}/d\bar{I}^2$, whereas the spectral response peaks at frequencies $\nu_R \lesssim 200$ GHz. Decreasing the resistance by burning-in of the contact, it was found that for underdamped contacts $\nu_R \propto R^{-1/3}$, almost independent of the junction geometry. Tapping the contact, i.e., changing the microscopic properties of the flat contact region (diameter, 5–10 μm), changed the absolute value of ν_R. Maximum resonant response occurred approximately for critical damping at $R = 80$–100 Ω. The observed behavior is interpreted as resonant detection at the plasma frequency. At low resistance values ν_R disappears, but additional resonances at $\nu > 150$ GHz appear, some of which could be identified as antenna resonances.

PACS numbers: 74.50.+r, 85.25.+k, 84.40.Jh

I. INTRODUCTION

Optimum coupling of external radiation to a Josephson junction detector is possible when the junction resistance equals the antenna resistance of the point-contact structure.[1] In practice this requires resistance of a few hundred Ohms, which also happens to be an optimum value for wide-band detection.[2] Stable niobium point-contact junctions that meet this requirement have been developed. A preliminary account of the current-voltage and response characteristics has been given before.[3] Here we report on the spectral response of these junctions to broad-band incoherent radiation. This work extends the classical study by Grimes, Richards, and Shapiro[4] on the spectral response of low-resistance Josephson junctions.

Low-resistance point contacts generally operate in the overdamped limit, where McCumber's damping parameter $\beta_c < 1$.[5] This parameter is defined by $\beta_c \equiv 2eI_cR^2C/\hbar$, where I_c is the maximum critical current, R is the normal-state resistance, C is the capacitance, e is the electron charge, and $2\pi\hbar$ is Planck's constant. At a constant value of the product I_cR, β_c increases linearly with R, so that the high-resistance junctions may operate in the underdamped limit ($\beta_c > 1$). For a typical niobium point contact C is 10^{-15} to 10^{-14} F,[3,6] and $I_cR \simeq 1300$ μV, so that the junctions will become underdamped at a resistance of 240 to 24 Ω. Due to the effect of intrinsic or external fluctuations the underdamped junctions show stable bias regions.[7] By a controlled burn-in process one can decrease the resistance of a point contact from, for example, 1 kΩ down to about 10 Ω, while the capacitance stays constant. In this way I have measured the spectral response as a function of junction resistance during the expected transition from underdamped towards overdamped.

In Sec. II the point-contact structure is described and the antenna properties are discussed. The experimental techniques to measure the current-voltage and response curves are described in Sec. III. General junction characteristics are presented in Sec. IV, whereas spectral response curves are given in Sec. V. In Sec. VI the resonance effects are related to the parameter β_c. A theoretical discussion of the effect of plasma oscillations on the spectral response is given in Sec. VII and a comparison is made with the experimentally obtained results.

II. JUNCTION STRUCTURE

A detailed description of the geometry of our point contacts has been given before.[3] In this section the antenna properties are discussed in connection with structural resonances of the response.

The detector geometry is shown schematically in Fig. 1. A 0.2-mm-diam niobium wire, bent into an L shape, is pressed with its sharpened end against a flat piece of niobium. The flat is soldered onto a leaf spring, which can be pulled towards a small electromagnet. The spring mounting results in very stable contacts, even at resistance values of 10 kΩ or more. The vibrational resonance occurs at about 1 kHz, which is sufficiently high to reduce the coupling to external vibrations. Contacts are made at 4.2 K. Because the niobium tip is stressed beyond the yield point, the contact area is flat with a diameter of 5—10 μm for the employed contact pressures (see also Ref. 3). The associated capacitance is estimated to be 10^{-15}—10^{-14} F. By light tapping one obtains a resistance value between 100 Ω and 10 kΩ. The resistance can be further decreased from these values by a burn-in process. For a junction voltage up to about 0.2 V the current-voltage characteristic is completely reversible, but in the range 0.3—0.6 V the junction breaks down (Fig. 2). By limiting the current one obtains another completely reversible characteristic (again up to 0.2 V) with a lower junction resistance. This burn-in process has been used to study the spectral response of a junction at different resistance values, without changing the capacitance of the contact.

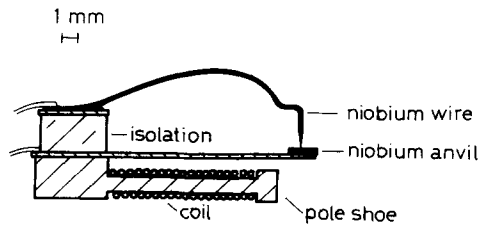

FIG. 1. Geometry of the point contacts.

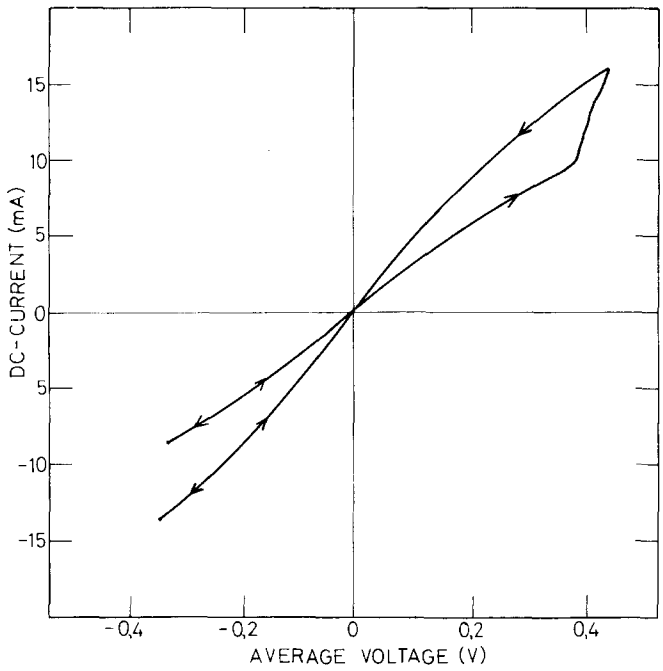

FIG. 2. Current-voltage characteristic showing burn-in of the point contact at about 0.4 V.

The niobium wire acts as an antenna, which induces a voltage across the junction when external radiation is applied. The employed structure acts as a long thin wire antenna with an antenna length l equal to the distance between the sharp point and the first bend.[8,9] In the presence of a ground plane, antenna resonances occur theoretically[10] at wavelengths of $\lambda \simeq 4l/(2n-1)$ with $n=1, 2, \ldots$, if the junction resistance $R \lesssim 37\ \Omega$; they occur at $\lambda \simeq 2l/n$ if $R \gtrsim 200\ \Omega$ and if the wire radius $a < l/40$. For $0 < l < \frac{1}{4}\lambda$ the reactance is capacitive, for $\frac{1}{4}\lambda < l < \frac{1}{2}\lambda$ inductive, and so on.

A travelling-wave solution is possible when the junction impedance is equal to the characteristic impedance of the antenna $|Z_k| = \zeta \ln(2l/a)$ with $\zeta \simeq 60\ \Omega$.[10] I have studied structures with $l = 1.2$ mm (series I) and $l = 2.5$ mm (series II, resulting in $|Z_k| = 190$ and $234\ \Omega$, respectively. Due to the fact that the ground plane does not extend to infinity but has dimensions on the order of the antenna length, $|Z_k|$ will in practice be higher (at most the double value). For junction resistances in the ranges 200—300 and 300—400 Ω, respectively, we then expect a travelling-wave behavior. Matarese and Evenson[8] concluded from the symmetry properties of their antenna patterns that their system behaved essentially as a travelling-wave antenna. Unfortunately, no information was given on the impedance values involved.

For an antenna length $l < \frac{1}{2}\lambda$, the radiation profile consists of a single lobe for a standing wave as well as for a travelling wave.[11] Efficient coupling of radiation is then possible by making use of a steep off-axis mirror, covering the radiation profile. For antenna lengths $l > \frac{1}{2}\lambda$ there is a lobe for each half-wavelength and the direction of the electric field reverses in each successive lobe. This reduces the maximum possible coupling (unless special phase plates are used). The studied structures therefore had optimum coupling to radiation with wavelengths longer than 2.4 and 5.0 mm, respectively.

III. EXPERIMENTAL TECHNIQUE

In Fig. 3 a schematic drawing is given of the experimental setup. The junction was mounted in the evacuated part of an all-metal helium Dewar. Radiation was focused directly on the junction by means of the ellipsoidal mirror with an $f/0.8$ beam through a 3-cm-diam TPX window. The radiation was chopped externally at a rate between 100 Hz and 1 kHz. All radiation with wavelength $\lambda < 400\ \mu$m was blocked to prevent heating of the detector. This was achieved by layers of CdO and PbO embedded in polyethylene,[12] a 2-mm-thick quartz filter, and 0.5 mm of black polyethylene. The junction was biased through a 10-kΩ wirewound resistor at 4.2 K from either a battery or a sweep generator. The ac voltage across the junction was amplified by a transformer (Triad JAF 2) at 4.2 K, surrounded by a superconducting shield. The JAF 2 was used unmodified; removal of the potting, as suggested in Ref. 13 for a similar transformer, resulted in strong microphonics. At room temperature the ac signal was further amplified by a low-noise amplifier (Brookdeal 5003). The total noise of this system as measured across a 100-Ω resistor at 4.2 K and at a frequency of 425 Hz was about $0.25\ \text{nV/Hz}^{1/2}$. At harmonics of 50 Hz the noise was significantly higher. The current through the junction was measured as the voltage across the bias resistor and this was fed into a dc differential amplifier (PAR 113); the dc detector voltage was amplified by another

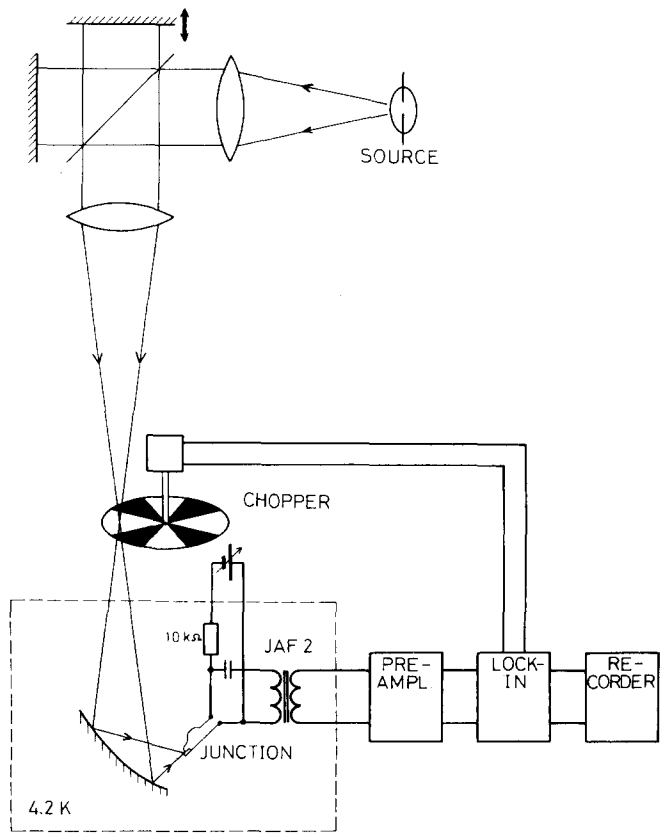

FIG. 3. Schematic drawing of the experimental setup.

differential amplifier (PAR 113). All leads going into the Dewar were heavily filtered by radio-frequency interference (RFI) feed-through filters, mounted in the wall of a connector box. The low-noise amplifier was kept within the shielded compartment; otherwise the 100-kΩ output impedance of the transformer would be shunted by the capacitance of the RFI filters. In this way external interference was completely eliminated even for junctions that coupled optimally to external radiation. Furthermore, the system was virtually free from electrical transients.

Spectral response measurements were performed with a Michelson interferometer (Grubb-Parsons), with a 100-μm-thick Mylar beamsplitter and a mercury arc as source. Radiation leaving the interferometer was focused on a chopper wheel at room temperature, placed in the outer focal point of the ellipsoidal mirror. The chopping frequency was, in general, 425 Hz, in the middle of the transformer range. The optical chopping

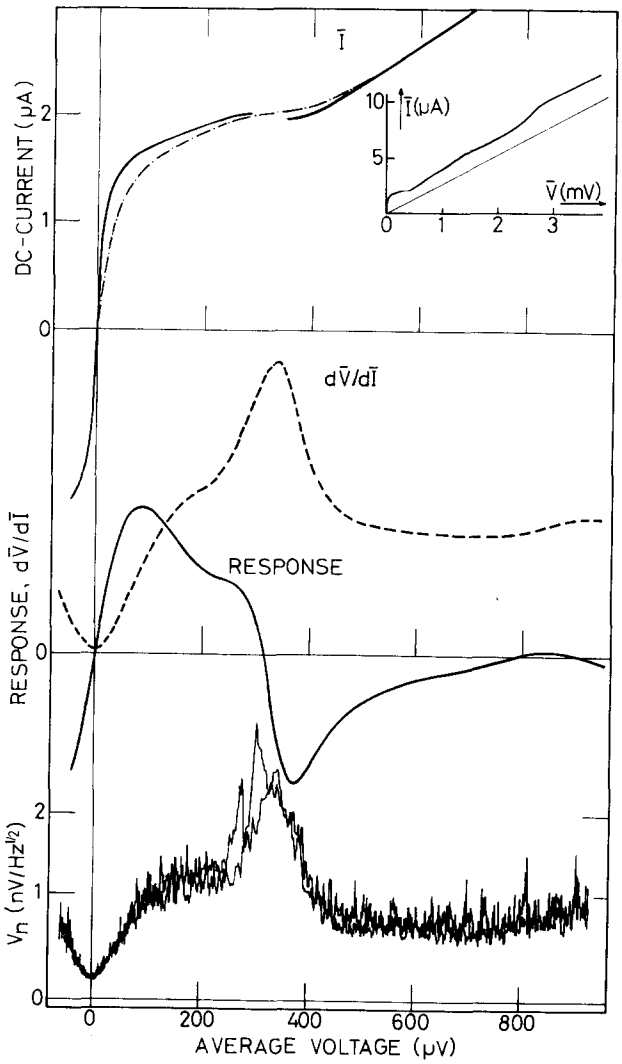

FIG. 4. Example of the current-voltage characteristic, the differential resistance, the response, and the noise voltage of a 400-Ω junction (see text). The noise voltage roughly follows the differential resistance. By dividing the squares of both quantities one obtains the spectral density of the current fluctuations, which follows an $\bar{I}/\bar{V}$ behavior. Lower impedance junctions generally show about a $1/f$ noise-power spectrum for frequencies between 100 and 1000 Hz.

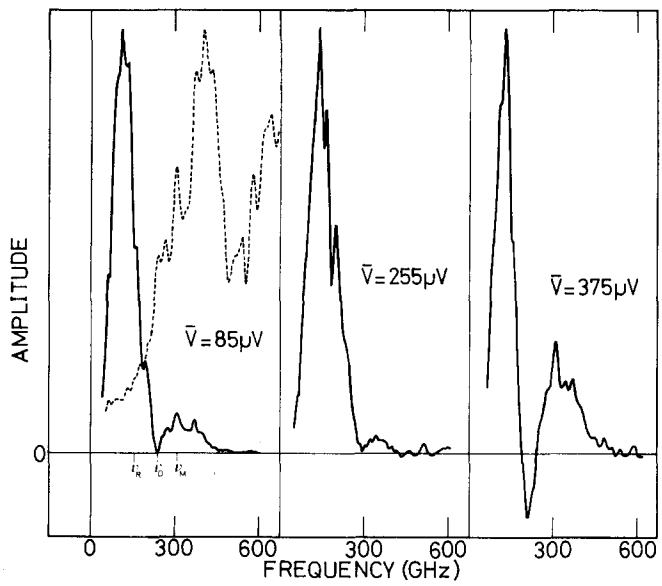

FIG. 5. Phase-corrected amplitude spectrum of the response to a mercury arc source of the junction of Fig. 4 at bias voltages corresponding to extrema in the response curve. The bolometer reference spectrum is dotted; for reasons of clarity no ratio spectra are given (see text). The amplitudes are normalized to unity.

efficiency was 25%. The amplified ac voltage was rectified in a lock-in amplifier and recorded as a function of the position of the movable mirror, driven by a stepping motor. The maximum displacement of this mirror was 2 cm, giving a spectral resolution of about 27 GHz (apodization included). The interferogram, obtained by this step-and-integrate method, was recorded on paper tape. Amplitude and phase Fourier transforms were computed by a PDP 11 computer. The accuracy and reproducibility of the peak positions in the spectra was ±7 GHz. Having completed a series of measurements, the Josephson junction was replaced by a 3-mm-diam silicon bolometer to obtain a reference spectrum. In some cases ratio spectra of the Josephson detector relative to the bolometer were determined. Because the response of the bolometer is a smooth function of the frequency, this eliminates the channel spectrum and other structure caused by the optical filters and the mercury arc source.

IV. GENERAL JUNCTION CHARACTERISTICS

In this section and Secs. V and VI a description is given of the various phenomena observed in the response of the studied contact structures. It is useful to start with an account of general characteristics of the junctions.

A current-voltage characteristic ($\bar{I}$-$\bar{V}$ curve) that was typical for junctions with $R > 100\ \Omega$ at $T = 4.2$ K is shown in Fig. 4. The drawn line is the $\bar{I}$-$\bar{V}$ curve with the window closed by a reflecting metal plate, so that a minimum of radiation was received by the detector. The inset shows the $\bar{I}$-$\bar{V}$ curve at voltages up to the gap voltage ($2\Delta/e$) at $\bar{V} \simeq 2.8$ mV. Gap and subgap structures are clearly visible. The resistance of the junction, defined as $d\bar{V}/d\bar{I}|_{\bar{V}>2\Delta/e}$, was 400 Ω. When a high level of 35-GHz radiation was applied to the junction the $\bar{I}$-$\bar{V}$ curve became a straight line with a resistance value

equal to $d\bar{V}/d\bar{I}|_{\bar{V}>2\Delta/e}$ to within 10% (see inset to Fig. 4). Therefore this value was taken as the normal-state resistance. For $\bar{V}>2\Delta/e$ almost all junctions show a current in excess of $\bar{V}/R$. This excess current is a characteristic feature of microbridges and has been explained by Likharev and Yakobson.[14] A hysteretic region is present at a current of about 2 μA. Removing the metal plate from the window and thus exposing the junction to 300 K blackbody radiation resulted in an $\bar{I}$-$\bar{V}$ curve indicated by the dotted line. The hysteresis has been quenched and the rounding off of the superconducting transition region has become stronger.

Closing the window by a gauze with a wire distance $d=0.5$ mm gave the original $\bar{I}$-$\bar{V}$ curve back, indicating that the observed change was due to radiation with $\lambda>2d=1$ mm (for these wavelengths the transmission of the gauze is negligible). On the other hand, closing the window by a mesh with a wire distance $d=8$ mm resulted in a dc response about 60% of that obtained with open window, so that the response had to be caused by radiation with $\lambda<16$ mm (the transmission of the mesh, integrated between 1 and 16 mm, is of the order of 50%). These tests exclude the possibilities that the response is due to heating of the contact or to high-frequency radiation from radio stations.

The $\bar{I}$-$\bar{V}$ curve resembles those calculated numerically by Kurkijärvi and Ambegaokar for underdamped junctions in the presence of a high level of thermal fluctuations.[7] The observed modification of the $\bar{I}$-$\bar{V}$ curve due to external radiation is similar to that found by Kanter and Vernon.[15] Illuminating a point-contact junction with the radiation of a gas-discharge tube ($\lambda<5$ mm), they also observed a rounding off of the superconducting transition region. In their case a fit to the data of Kurkijärvi and Ambegaokar was possible for $\beta_c=1$.

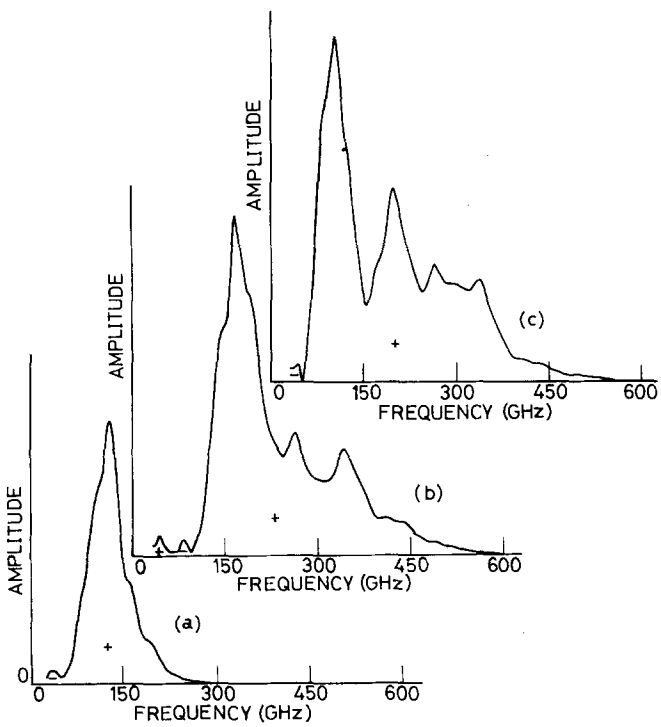

FIG. 6. Amplitude spectra of Josephson junctions from series IB relative to a silicon bolometer, biased at maximum response; (a) $R=100\ \Omega$, (b) $R=26\ \Omega$, and (c) $R=17\ \Omega$. The sign indicates the phase of the response.

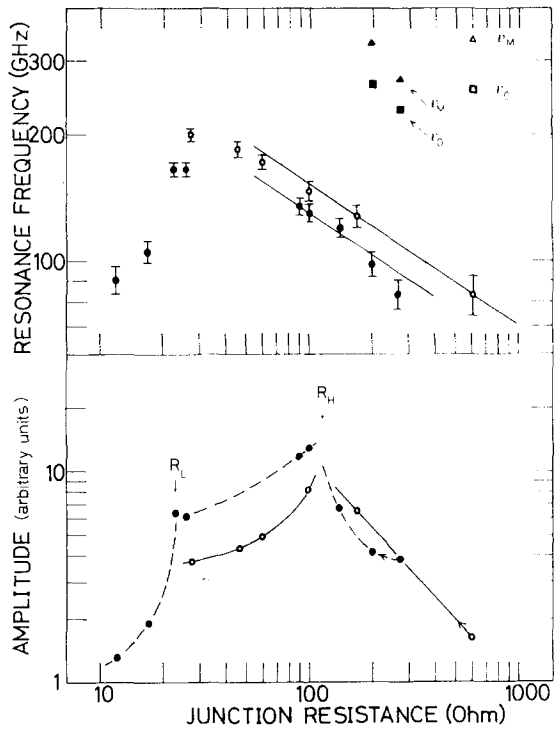

FIG. 7. Junction with an antenna length of 1.2 mm (series I). Plot of the frequency of the peak response and its amplitude versus the junction resistance R. In this series R was first reduced from 620 to 28 Ω by burn-in (I A, circles), then a new setting of the contact was achieved by tapping, after which R was again reduced from 270 to 12 Ω by burn-in (I B, dots). The spectral features ν_0 and ν_M are defined in Fig. 5.

Figure 4 also shows the ac voltage response obtained by chopping room-temperature radiation at a frequency of 425 Hz. The detector alternatively saw the atmosphere, with an estimated emissivity of about unity, and the back side of the chopper, with a reflection coefficient of about unity for $\lambda\gtrsim1$ mm. In this way the effective temperature difference as seen by the detector should be about 300 K; the measured $\bar{V}_{rms}=4.3$ μV. The response was not due to reflection against the chopper of radiation emitted by the detector itself, as suggested by Grimes, Richards, and Shapiro[4] and found experimentally by Ulrich and Kluth.[16] A small axial displacement or inclination of the chopper wheel did not affect the response. As another check, I measured the response to a polystyrene cup filled with water and placed directly behind the chopper wheel, at two different temperatures above and below room temperature. A positive and negative signal were obtained, respectively, with $\bar{V}_{rms}/\Delta T=12.7$ nV/K. Because the radiative energy of a source at 300 K, emitted between 1 and 16 mm wavelength, is about proportional to the temperature, room-temperature radiation should give a signal of about 3.8 μV. This is practically 90% of the measured signal.

Maximum response occurs at an average voltage $\bar{V}=85$ μV. Just above the quenched hysteretic region at $\bar{V}=375$ μV a strong negative response (i.e., a de-

crease in voltage) is observed. Below this region at $\bar{V}=255$ μV we find a local maximum. Choosing the bias current at these three characteristic points, the response to the mercury arc source was spectrally analyzed with the Michelson interferometer (Fig. 5). The bolometer reference spectrum has been indicated by the dotted line. In both spectra we observe channeling[17] with a period of about 30 GHz, due to interference effects in the quartz filter and/or the quartz envelope of the mercury arc source. For $\nu < 100$ GHz the signal-to-noise ratio with the bolometer was too small ($\lesssim 2$) to remove these features in the ratio spectrum and therefore no ratio spectrum is shown.

The response at $\bar{V}=85$ μV peaks at $\nu=110$ GHz. Below $\bar{V}=h\nu/2e \simeq 220$ μV the integrated response is predicted to follow $d\bar{V}/d\bar{I}$,[18] but Fig. 4 shows that this is not the case. Instead maximum response occurs at a voltage below that of the local maximum in $d\bar{V}/d\bar{I}$, almost corresponding to a maximum of $d^2\bar{V}/d\bar{I}^2$. This behavior is found to be characteristic for detection at a high fluctuation level.[3] For strongly damped junctions this has been predicted in Ref. 19, but it is apparently true also for the underdamped junction of our example (see Sec. VIII). From Fig. 5 we see that the response at $\bar{V}=375$ μV is mainly due to radiation with $\nu < 2e\bar{V}/h$, in which case detection of a Josephson junction is classical, i.e., the response follows $d^2\bar{V}/d\bar{I}^2$. This explains the negative sign of the integrated response. From the phase spectrum I find that the spectral response changes sign at $\nu=2e\bar{V}/h$, as expected. Biasing at a higher voltage shifted this frequency accordingly. A remarkable feature is the zero response at 250 and 300 GHz for the bias points $\bar{V}=85$ μV and $\bar{V}=255$ μV, indicated in Fig. 5 by ν_0.

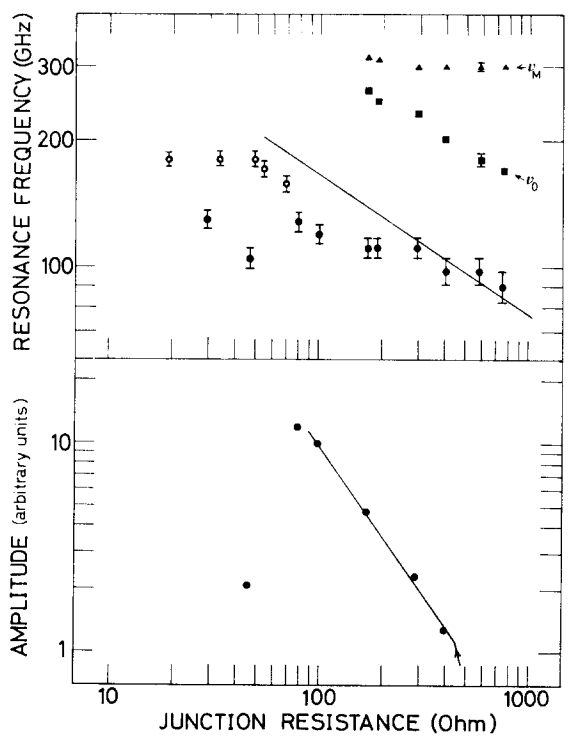

FIG. 8. As Fig. 7 but for a junction with an antenna length of 2.5 mm (series II). The first burn-in went from 750 to 30 Ω (II A, dots) the second from 70 to 19 Ω (II B, circles). At about 110 GHz we may observe pulling towards a geometrical resonance.

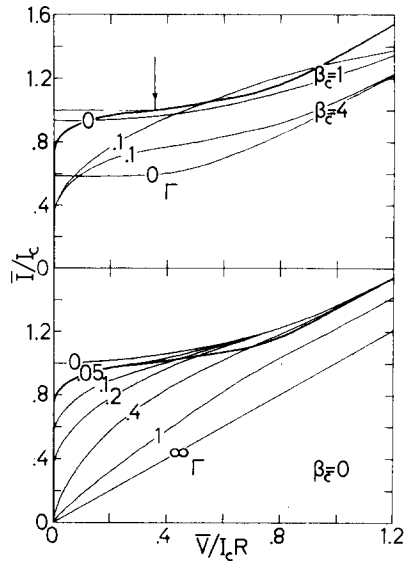

FIG. 9. Comparison of current-voltage characteristics of a typical lightly damped (50 Ω) junction (heavy curves) with computed characteristics (light curves). The measured differential resistance around 1 mV has been equated to R; the excess current (Sec. IV) should be subtracted. The upper half compares with computations by Kurkijärvi and Ambegaokar (Ref. 7) for two values of the damping parameter β_c without noise ($\Gamma=0$) and with some noise ($\Gamma=0.1$). The arrow indicates the bias voltage at which no response is measured; the corresponding current I_{c0} is close to I_c (Sec. VI). The lower half compares with computations by Ambegaokar and Halperin (Ref. 26) with strong damping ($\beta_c=0$) at various noise levels Γ (Sec. VII).

V. SPECTRAL RESONANCES

The main feature in the spectral response curves is the strong peak at one particular frequency. This response is not due to a high-frequency cutoff at $(RC)^{-1}$ caused by the instrumentation. From the expected mean capacitance value of 3×10^{-15} F, we calculate a cutoff at 1000 GHz, which is an order of magnitude higher than measured. On the other hand, according to the expected resonance frequencies neither the antenna length nor any other characteristic dimension, e.g., the distances between the point and the various sides of the anvil, can be related with this peak response. Five structures with completely different antenna lengths were investigated and in all the 50 cases with $R \geq 100$ Ω a peak response was found at a frequency between 80 and 200 GHz. In one special case the largest antenna dimension was 0.5 mm so that for an eventual antenna resonance in any case $\nu_R \geq 150$ GHz ($\frac{1}{4}\lambda$ resonance). But at 240 Ω, where either a travelling-wave response (nonresonant) or a $\frac{1}{2}\lambda$ resonance at $\nu \geq 300$ GHz was expected, a peak response occurred at 83 GHz. For $R > 300$ Ω, the peak responses always occurred below 150 GHz.

Because of the strong suggestion that the peak response is related to some other kind of resonance, it will be further discussed as if it were a resonance. Investigating its properties, I found that the resonance frequency increased while decreasing the resistance by burning-in of the contact. As described earlier, this

method allows one to vary the resistance and the critical current of the junction at a constant capacitance. Figure 6(a) shows the spectral response of a junction of 100 Ω relative to a 3-mm bolometer, obtained by the burning-in of a junction of initially 270 Ω. The resonance frequency has shifted from an initial value of 85 to 130 GHz and at the same time the resonance amplitude increased. Figure 7 shows the dependence of the resonance frequency and amplitude on R for a junction structure with an antenna length of 1.2 mm (series I). For $R > 200$ Ω the values of ν_0 and ν_M (compare with Fig. 5) have been indicated. When the resistance was decreased further, strong submillimeter response began to develop. The resonance frequency still increased but the amplitude decreased. Maximum ν_R was observed at 26 Ω with $\nu_R = 170$ GHz. The spectral response at this point is shown in Fig. 6(b). Below this resistance value both resonance amplitude and frequency decreased. The response of a junction with $R = 17$ Ω is shown in Fig. 6(c).

In Figs. 6(b) and 6(c) we see clear subsidiary resonances. They occurred at frequencies of 200, 260, and 330 GHz that did not shift with resistance and probably correspond to $\frac{3}{4}\lambda$, λ, and $\frac{5}{4}\lambda$ resonances of the antenna. From these frequencies we get an effective antenna length of 1.15 mm, to be compared with a physical length of 1.2 mm. Another burn-in series with the same structure (series IA, circles) is also shown in Fig. 7 (the 270-Ω junction of series IB was obtained by tapping the 28-Ω junction of series IA). The dependence of frequency and amplitude on the resistance is qualitatively the same. The absolute response level, however, is considerably smaller.

Figure 8 shows the dependence of the resonance frequency and amplitude on R for a different structure with an antenna length of 2.5 mm (series II). Especially the zero response at ν_0 and the local maximum at ν_M, which occurred for $R \gtrsim 200$ Ω, were measured in detail. We see that ν_M is approximately constant, while ν_0 increases with decreasing resistance until $\nu_0 \simeq \nu_M$, after which both tend to increase and finally disappear at $R = 80$ Ω with maximum resonant response. The sudden decrease of the resonance frequency and amplitude by burning-in from 80 to 46 Ω is accompanied by a drastic change in the $\bar{I}$-$\bar{V}$ curve. A sharp transition appears from the superconductive region to the resistive region. The latter starts with a relatively low differential resistance and the gap and subgap structures have almost disappeared. This is often observed for low-impedance point contacts. It has been pointed out that such a characteristic can be caused by multiple contacts with different values for the critical current.[20] The low-impedance junctions obtained by the burn-in method nevertheless showed no effect of a magnetic field on the critical current, contrary to low-impedance junctions obtained by tapping with the electromagnet. For the maximum field generated of about 100 G not the slightest effect on the response at the bias point with maximum differential resistance could be detected.

Considering the amplitude of the peak response, plotted in Figs. 7 and 8, we can distinguish between three resistance regions, separated by the transition values R_L and R_H. For series IB these are 23 and 100 Ω, respectively. Above R_H the response is resonant with a half-width of about 75 GHz. Below R_H submillimeter response is important and antenna resonances occur. Below R_L the $\bar{I}$-$\bar{V}$ curve is characteristic for a strongly damped junction with a relatively low $I_c R$ product, while the resonance frequency decreases with the resistance and finally disappears.

VI. RELATION WITH THE DAMPING

Because of the apparent importance of the junction resistance for the character of the resonance, it is useful to discuss the possible relation through the parameter $\beta_c \equiv 2eI_c R^2 C/\hbar$. We therefore need to know the critical current I_c. For junctions with $R \gtrsim R_H$, where the $\bar{I}$-$\bar{V}$ curve is rounded off by external radiation and intrinsic thermal fluctuations, I_c can be estimated by comparing the measured curves with curves computed by Kurkijärvi and Ambegaokar.[7] In Fig. 9 it is shown that, if the junction is about critically damped ($\beta_c = 1$), the curves computed without and with some noise intersect at a current close to I_c. There will be no response at the intersection, because external radiation acts as thermal noise. (This is strictly true for $\bar{V} < h\nu/2e$ only; for higher voltages the radiation averages the $\bar{I}$-$\bar{V}$ curve, which also results in a negative response.) For lightly underdamped junctions the experimentally determined bias current I_{c0}, where the response is zero, will therefore correspond to about I_c. This is in agreement with the experimental results of Kanter and Vernon.[15] It follows from Fig. 9 also that the intersection occurs for a smaller current when $\beta_c > 1$. This implies that for high-resistance junctions I_{c0} will be an underestimate of I_c.

In Fig. 10, I_{c0} is plotted versus R for the junctions of series I and II. We see that, for $R_L < R < R_H$, the prod-

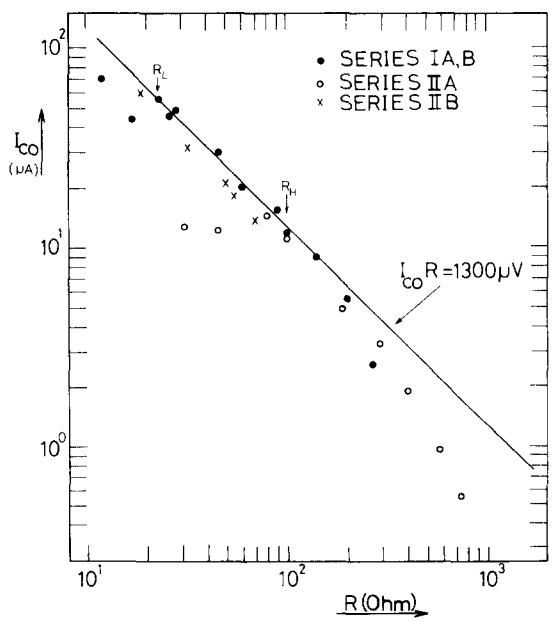

FIG. 10. Plot of the bias current at zero response I_{c0} versus the resistance R. The higher resistance values of series I A have not been measured.

uct $I_{c0}R$ is about constant at 1300 μV, but for $R > R_H$ there is a downward deviation. This makes it likely that maximum resonant response (at $R = R_H$) approximately corresponds with the condition for critical damping.

To illustrate this point further, I want to discuss examples of the spectral response of junctions for which $R \lesssim R_H$ and $R \gtrsim R_H$. In Fig. 11 pertinent data are shown for a junction with $R = 50\ \Omega$ just below R_H. The $\bar{I}$-$\bar{V}$ curve shows cusplike features at about $\bar{V}_1 = 2\Delta/e$, $\bar{V}_2 = 2\Delta/2e$, and $\bar{V}_3 = 2\Delta/3e$ with $2\Delta/e = 2.55$ mV. The response to the mercury lamp shows maxima corresponding to the maxima of $d^2\bar{V}/d\bar{I}^2$, but is not proportional to $d^2\bar{V}/d\bar{I}^2$, especially not at the higher voltages. The spectral response was determined at the five indicated bias points. At maximum response ($\bar{V}_{max} = 60$ μV) the one broad peak is typical for all junctions with $R \lesssim R_H$. At minimum response ($\bar{V}_{min} = 500$ μV) the response changes sign at about 260 GHz, which is to be compared with $2e\bar{V}/h = 240$ GHz. Although the zero response occurs at a slightly higher frequency than expected, it did nevertheless shift with bias voltage, as for the junction in Fig. 5. (For a high-fluctuation model this is predicted in Ref. 19.) The amplitude spectrum at $\bar{V} = 900$ μV just above $\bar{V}_3 = 2\Delta/3e$ shows zero response at 430 GHz, while $2e\bar{V}/h = 434$ GHz. The spectrum at $\bar{V}_2 = 2\Delta/2e = 1250$ μV has a singular response

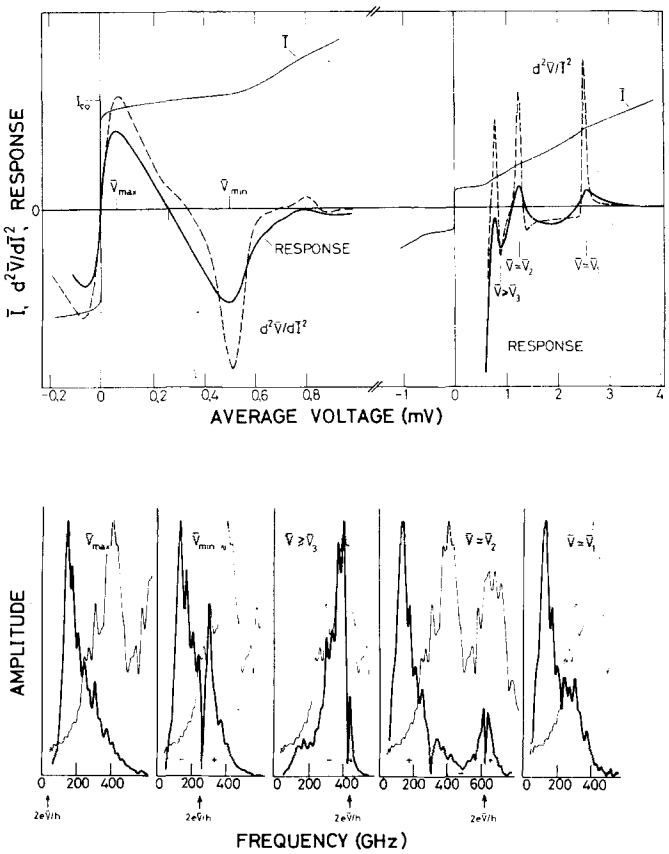

FIG. 11. Current-voltage characteristic, its second derivative, and response of a 50-Ω junction and spectral response of this junction at the indicated bias voltages. To retain details, the direct spectra (heavy curves) are shown together with the reference spectra (light curves); the amplitudes have been normalized to unity. Peak response occurs at 150, 135, 405, 140, and 130 GHz, respectively.

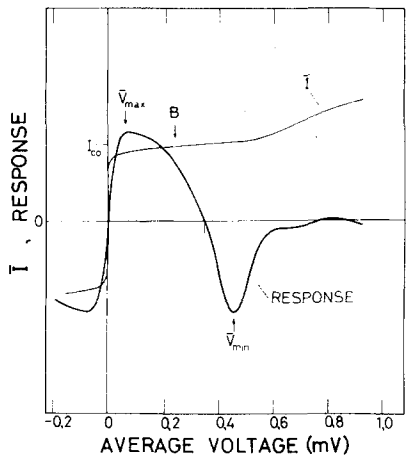

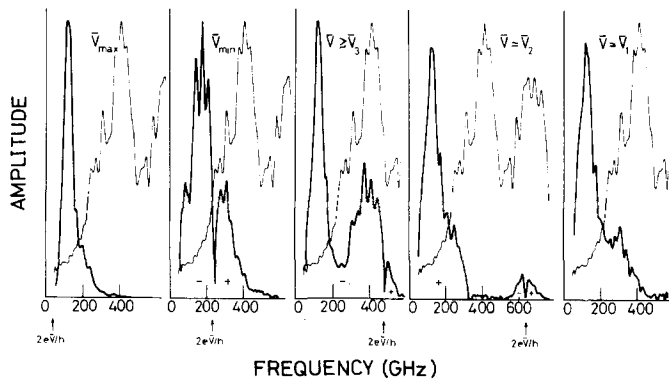

FIG. 12. Current-voltage characteristic and response of a 100-Ω junction from series II A; spectral response of this junction at the indicated bias voltages (see also Fig. 11). Peak response occurs at 120 GHz except for $\bar{V}_{min}$, which shows a submaximum there.

at 618 GHz, while $2e\bar{V}/h = 603$ GHz. Remarkable is another sign reversal at about $e\bar{V}/h$. At the gap voltage $\bar{V}_1 = 2\Delta/e$ no singularity was measured at the corresponding frequency of 1236 GHz. This actually proves the effectiveness of the optical filters, which blocked all radiation with $\nu > 750$ GHz to avoid aliasing in the spectra.[17]

A different behavior is found for a junction from series II A with $R = 100\ \Omega$ just above R_H (Fig. 12). The resonance at maximum response is relatively sharper, with a half-width of 60 GHz (uncorrected for the finite resolution of the interferometer of 27 GHz). At a bias point B above $\bar{V}_{max}$, on the broad maximum of the $\bar{I}$-$\bar{V}$ curve, we again observe a local zero, just like for the junction of Fig. 5. At the higher bias voltages we find a relatively weaker submillimeter response. The most remarkable difference with the spectra of Fig. 11 is the persistence of the resonant response at about 120 GHz, for all the bias voltages.

Information on a possible dependence of ν_R on I_c can be gained by either increasing the temperature or applying a magnetic field, so that I_c is reduced. Unfortunately, with the system used the former was not possible, whereas the latter required a stronger field than could be realized. However, in one particular junction with

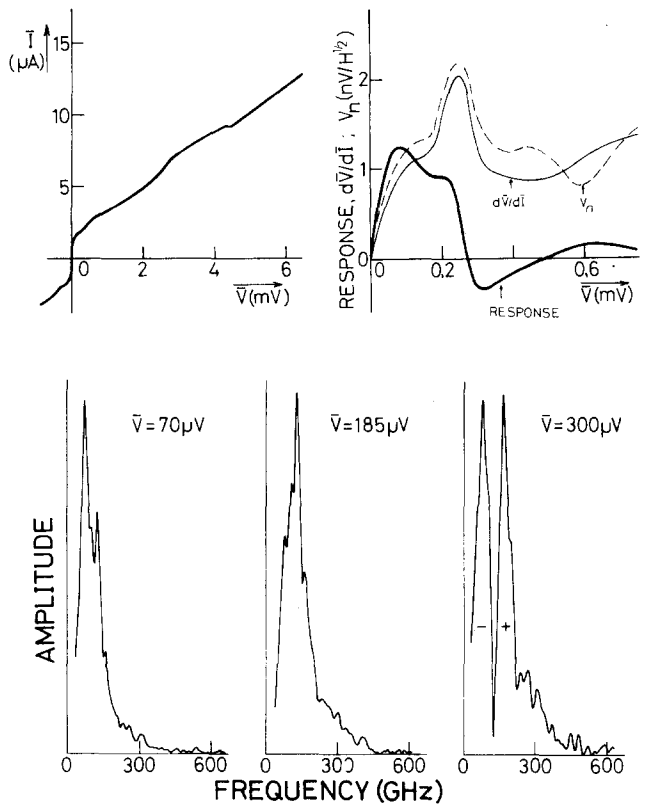

FIG. 13. Example of a deviating behavior for high-resistance junctions (see text).

$R = 60\ \Omega$ and $I_{c0} \simeq 8\ \mu$A, obtained by tapping, the available magnetic field could reduce the critical current to about 0.65 of the initial value. The spectrum at maximum response was relatively the same as that of Fig. 11 but with a slightly higher submillimeter response. In this case the resonance frequency was reduced from 135 to 116 GHz. Though this one experiment may not be significant, it contains the hint that ν_R is rather sensitive to I_c.

In a few cases a deviating $\bar{I}$-$\bar{V}$ curve occurred for $400 < R < 600\ \Omega$. An example is given in Fig. 13 for a junction with $R = 560\ \Omega$. An additional bump is present above the "supercurrent", while beyond the gap voltage a small hysteretic region is present. The response approximately follows $d^2\bar{V}/d\bar{I}^2$ and the current noise $\bar{V}_n/(d\bar{V}/d\bar{I})$ shows unexpected extrema at $\bar{V} = 450$ and 600 μV. Spectral measurements at the different response maxima indicate a remarkable shift of the resonance frequency from 75 GHz at the first maximum to 130 GHz at the second maximum (compare Fig. 5). By lightly tapping the contact, the resistance could be lowered. The hysteretic region moved towards a higher current and a lower voltage, suggesting a constant power dissipation. Possibly this latter phenomenon is due to heating.

The low-resistance junctions ($R \lesssim 20\ \Omega$) often showed considerable structure in their response curves. These features became particularly pronounced at lower temperatures. Figure 14 shows the spectral response, biased on a response peak, for $T = 1.8$ K. The response is a singular with a sign reversal at $\nu \simeq 2e\bar{V}/h = 350$ GHz, which probably corresponds to a $\frac{1}{4}\lambda$ antenna resonance. By cooling from 4.2 to 1.8 K the critical currents of the low-impedance junctions increased by about 20%, compared with about 10% for junctions with $R > 20\ \Omega$. The latter is about equal to what is expected theoretically.[21] Some of the low-impedance junctions showed an almost hysteretic bias region just above the critical current, of the same type as was studied by Grimes, Richards, and Shapiro.[4] The spectral response was similar to what they found, i.e., an oscillating response as function of the frequency. In the present case, however, the period was higher (about 1100 GHz) and the response extended to wavelengths of at least 40 μm, far beyond the cutoff of the optical filters (400 μm). Therefore in the present case this type of response behavior was an experimental artifact. Similar observations have been reported in the literature,[22] and indicate that one should be careful with the interpretation of harmonic effects. In Fig. 14 for example, a singular response seems to be present also at the second harmonic of 350 GHz. This feature is even more clearly observed in the cosine Fourier transform, but is probably not real.

VII. INTERPRETATION OF THE SPECTRAL MEASUREMENTS

We have to account for the dependence of the resonance frequency ν_R on R. Let us first investigate the dependence, predicted by the geometrical resonance of the discoidal region, formed by the flattened top of the pointed wire and the flat electrode. Assume a model with a mean electrode separation t and a mean disk radius r, which is much larger than the radius a of one single bridge between the electrodes. The resonance frequency $\nu_R = (2\pi)^{-1}(LC)^{-1/2}$ can be estimated from the inductance L and the capacitance C of the disk. As long as $r \ll \lambda_R = c/\nu_R$, L and C may be considered to be lumped parameters; this is the case, because $r \simeq 4\ \mu$m and $\lambda_R \simeq 2$ mm. If the thickness t is much larger than the magnetic penetration depth, $L = (\mu/2\pi)t \ln(r/a)$ with μ the permeability,[6] which can be equated to the vacuum value μ_0. Furthermore, $C = \pi\epsilon(r^2 - a^2)/t$ with ϵ the permittivity, which can be equated to the vacuum value

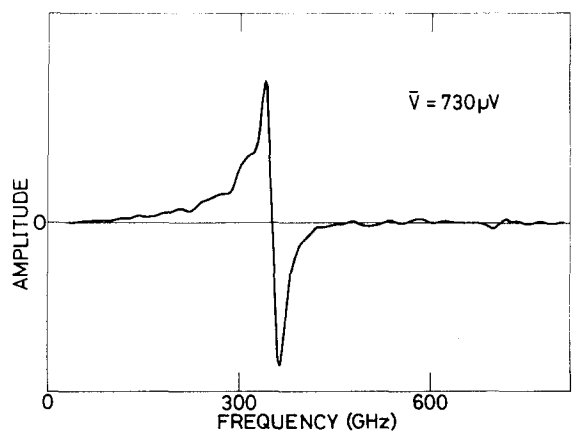

FIG. 14. Phase-corrected amplitude spectrum of the response of a junction with $R = 5.8\ \Omega$, biased on a response maximum at $\bar{V} = 730\ \mu$V.

ϵ_0, whereas $r^2 - a^2 \simeq r^2$. So the resonance frequency is

$$\nu_R = \frac{1}{2\pi} \frac{2^{1/2} c}{r \ln^{1/2}(r/a)} . \quad (1)$$

One can estimate a from R and the specific resistance ρ of niobium ($\simeq 10^{-8}\ \Omega$ m).[6] In the short mean free path limit $R = \rho/(2a)$,[23] so that for $R \simeq 100\ \Omega$, $a \simeq 0.5$ Å. The corresponding resonance frequency is about 5000 GHz, which is more than one order of magnitude higher than observed. Although t might be smaller than the magnetic penetration depth, resulting in a lower value for ν_R, the same dependence $\nu_R \propto \ln^{-1/2}(R)$ applies, which is much slower than was found experimentally. Therefore the model of an increasing bridge diameter cannot explain the observed frequency shift with decreasing resistance. Moreover, it also fails to explain the interesting observation that ν_R is rather sensitive to I_c.

We are therefore led to the conclusion that the observed resonance effects are intrinsic to the Josephson current and that the resonance amplitude and frequency depend on the damping parameter β_c. Let us investigate what happens when a junction is biased below the critical current, in the presence of thermal fluctuations. The potential energy of the junction as a function of the phase difference ϕ shows local minima and maxima.[24] If at some moment the system is at a mininum (the case of a phase lock), it can escape from it by thermal fluctuations. The phase then rotates until it is recaptured in the next potential well, and from $V = (\hbar/2e)(d\phi/dt)$ we see that a finite voltage is developed across the junction. The rate at which the system escapes has been given by Chandrasekhar[25] for the related problem of Brownian motion.[26] One obtains for the angular attempt frequency

$$\omega_A = (\tfrac{1}{4}\eta^2 + \omega_J^2)^{1/2} - \tfrac{1}{2}\eta, \quad (2)$$

where $\eta = (RC)^{-1}$ is the damping factor and $\omega_J = \omega_{J0}\cos^{1/2}(\phi_0)$ is the angular frequency corresponding to the curvature at the bottom and the top of the potential; ϕ_0 is the thermal average of ϕ and the Josephson plasma frequency $\omega_{J0} = (2eI_c/\hbar C)^{1/2}$. External radiation will enhance escape over the potential barrier with a resonance frequency $\nu_R = \omega_A/(2\pi)$. Using the definitions of β_c and η, expression (2) can be rewritten as

$$\frac{\omega_A}{\omega_c} = \left(\frac{1}{4\beta_c^2} + \frac{\cos(\phi_0)}{\beta_c}\right)^{1/2} - \frac{1}{2\beta_c} \quad (3)$$

with $\omega_c = 2eI_cR/\hbar$. For a constant I_cR product, as appears to be the case (Fig. 10), and a constant C, $\beta_c \propto R$, so that Eq. (3) virtually gives the resonance frequency as a function of the resistance. For $\cos(\phi_0) = 1$ the behavior of Eq. (3) is shown in Fig. 15. We see that ω_A is a slowly varying function of β_c. For large values of β_c, i.e., for light damping, the asymptotic solution is $\omega_A/\omega_c = [\cos(\phi_0)/\beta_c]^{1/2} = (\beta_c)^{-1/2}$ and for small values of β_c, i.e., for heavy damping, $\omega_A/\omega_c = \cos(\phi_0) = 1$. These solutions correspond to the plasma frequency ω_J and the frequency ω_c, respectively. Aperiodic damping[25] of the phase oscillations sets in at the critical value $\beta_c = \frac{1}{4}$. An increase of $\bar{I}$ towards I_c shifts this onset to higher values of β_c according to the relation $\beta_c = [4\cos(\phi_0)]^{-1}$, where $\cos(\phi_0) \simeq (1 - x^2)^{1/2}$ with $x = \bar{I}/I_c$. Note that the above condition for critical damping refers to the phase oscillations in a potential well. It differs from the condition for a rotating phase solution at $\beta_c \simeq 0.8$,[5] which is also called critical.

Let us study the behavior of $\cos(\phi_0)$ in order to see how the above asymptotic solutions depend on R at the bias point with maximum response. Experimentally we find that maximum response occurs at $\bar{V} \lesssim 100\ \mu$V, while $\nu_R \gtrsim 75$ GHz, so that $\bar{V} < h\nu_R/2e$. Therefore the response is proportional to $d\bar{V}/dT^*$, where T^* is the effective temperature to which the junction is raised by external radiation. At heavy damping the relation between $\bar{V}$ and T^* can be approximated by the thermal activation model over a potential barrier with height ΔE, giving[27]

$$\bar{V} = I_cR \exp(-\Delta E/kT^*), \quad (4)$$

which is applicable for $\bar{V} \lesssim 0.2 I_cR$ and $\Delta E \gtrsim 2kT^*$ (k is Boltzmann's constant). Maximizing the response, i.e., solving $d^2\bar{V}/dT^{*2} = 0$, one finds $\Delta E = 2kT^*$. At light damping one can expect that the condition for maximum response will not be much different from $\Delta E = 2kT^*$. The only difference is that in this case the phase will be continuously retrapped in a potential well, so that the system behaves as a drifting (rather than as a fixed) oscillator. Although the following calculation will be strictly valid for heavy damping only, it is probably valid for light damping, as well.

Following Fulton[28] we now approximate the barrier height by $\Delta E \simeq (\hbar I_c/2e)\frac{2}{3}(2 - 2x)^{3/2}$. Using the condition for maximum response this is equivalent to

$$1 - x \simeq \tfrac{1}{2}(3\Gamma)^{2/3}, \quad (5)$$

where $\Gamma \equiv kT^*/(\hbar I_c/2e)$. For $\cos(\phi_0) \simeq (1 - x^2)^{1/2} \simeq [2(1 - x)]^{1/2}$ it follows that

$$\cos(\phi_0) \simeq (3\Gamma)^{1/3}, \quad (6)$$

Because $\Gamma \propto 1/I_c$ and for a constant I_cR product $I_c \propto 1/R$, this results in $\cos(\phi_0) \propto R^{1/3}$, so that the asymptotic solutions of Eq. (3) become

$$\omega_A/\omega_c = [\cos(\phi_0)/\beta_c]^{1/2} \propto R^{-1/3} \quad (\beta_c \gg 1) \quad (7)$$

$$\omega_A/\omega_c = \cos(\phi_0) \propto R^{1/3} \quad (\beta_c \ll 1). \quad (8)$$

Both regimes are connected by a shallow maximum around $\beta_c \simeq 1$. The straight lines in Figs. 7 and 8 correspond to Eq. (7). We find a fair agreement at large resistance values as well as a deviation at low resistance

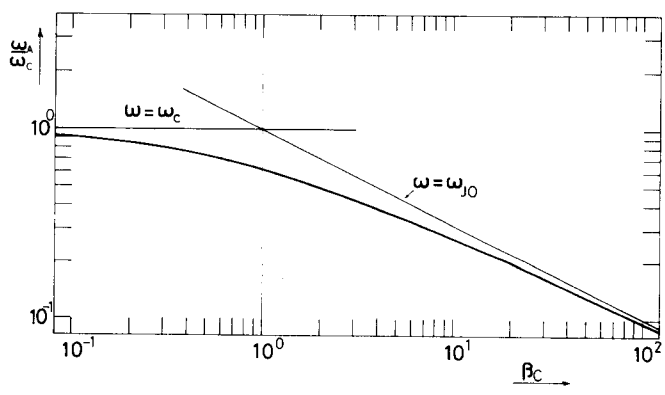

FIG. 15. Behavior of Eq. (3) for $\cos(\phi_0) = 1$.

values, which in the case of series II B seems to confirm the shallow maximum. Because for heavily damped junctions maximum response occurs at $\bar{I} > I_c$, the regime described by Eq. (8) will not be entered. The difference in resonance frequencies between series I A and I B at high resistance values can now be ascribed to a small difference of the capacitance caused by the tapping. I will return to this point. The maximum resonance frequency in series II B of 180 GHz can be compared with an estimate based on the above theory. By comparing the $\bar{I}$-$\bar{V}$ curve of the 50-Ω junction in series II B with computed curves, we estimate $\Gamma \simeq 0.05$ (Fig. 9). The attempt frequency is then characterized by $\cos(\phi_0) = (3\Gamma)^{1/3} \simeq 0.53$ and $\beta_c = [4\cos(\phi_0)]^{-1} \simeq 0.47$. From Eq. (3) it follows that the resonance occurs at $\omega_A/\omega_c \simeq 0.44$. In the case of series II B the $I_{c0}R$ product is constant at 1000 μV (Fig. 10), so that $\nu_c = \omega_c/2\pi \simeq 510$ GHz. The predicted resonance frequency is 225 GHz or only 25% higher than observed, which gives confidence in the correctness of this interpretation.

It follows that the main response in the junctions is due to a plasma mode and not to a geometrical mode. This explains the similar frequencies of the main resonance in two very different geometries (Figs. 7 and 8). Antenna modes are observed, however, and cause some of the structure in the submillimeter response. When the plasma mode is heavily damped, the geometrical modes become relatively more important (sequence in Fig. 6). Plasma oscillations do not depend on the external geometry but their coupling to external fields does.[29] It is likely that the large difference in the maximum response between the junctions from series I A and I B has to do with a small difference in the physical contact. That the difference is small can be inferred from the unchanged $I_{c0}R$ product (Fig. 10) and the modest increase of C after tapping. But at maximum response the coupling of the plasma mode to external radiation is about twice as good after the tapping. Apparently geometrical changes on a microscopic scale can significantly enhance the overlap of the spatially varying external field and the uniform plasma field between the electrodes.

The sudden change in appearance of the $\bar{I}$-$\bar{V}$ curve below R_L (Fig. 7; see Sec. V) is probably due to changes in the microscopic nature of the bridge (or bridges). The rapid decrease of ν_R indicates that the bias current for maximum response is shifting towards I_c and above, so that the plasma frequency becomes zero. In this case probably only antenna resonances will be excited. The peak response at these resonances, however, is much smaller than the maximum response at the frequency of the critically damped plasma resonance.

Finally, it should be stressed that the theoretical basis of the above interpretation is weak. First, there is no firm proof that $\Delta E = 2kT^*$ for light damping (although for any $\Delta E \propto kT^*$ the $\nu_R \propto R^{-1/3}$ relation results). Second, Eq. (2) is strictly valid only for $\Delta E > 2kT^*$ and, third, no phase-dependent conductivity is taken into account, which gives nonlinear damping and will result in a different value for β_c at critical damping. Finally, quantum effects in the response may be important because in many of the studied contacts $h\nu_R \simeq 2kT^*$. A thorough computational study of the differential equations describing the junction is clearly needed, but is not yet available.

VIII. SUMMARY

A description is given of niobium point-contact Josephson junctions, which are well suited for broadband detection of mm radiation. The antenna characteristics of the structures employed are discussed. Using a Michelson interferometer the spectral response has been determined for two series of junctions, each of which consisted of a number of contacts with continuously decreasing resistance. These were achieved by a controlled burn-in, such that in each series the capacitance and the I_cR product remained constant. With this method the characteristic resonance of the response could be related to plasma oscillations in the Josephson current and to their damping. Other possible causes are investigated but had to be discarded. In some cases subsidiary resonances could be related to the antenna structure. A theory is given of the dependence of the resonance frequency ν_R on the junction resistance R, which predicts an asymptotic behavior $\nu_R \propto R^{-1/3}$ for underdamped junctions and a rather constant ν_R when the oscillations become overdamped. This theory fits the measurements. The response peaks for critically damped junctions with $R \sim 100$ Ω at $\nu_R \sim 150$ GHz. A number of associated effects are qualitatively discussed.

LIST OF SYMBOLS

β_c	$2eI_cR^2C/\hbar$
Γ	$2ekT^*/(\hbar I_c)$
Δ	energy gap
ΔE	height of energy barrier
ϵ	permittivity
η	damping frequency $(RC)^{-1}$
λ	wavelength
μ	permeability
ν	frequency
ν_0	frequency at zero response (Fig. 5)
ν_A	attempt frequency
ν_M	frequency at subsidiary response (Fig. 5)
ν_R	frequency at main response (Fig. 5)
ρ	specific resistance
ϕ	phase difference in order parameter
ϕ_0	thermal average of ϕ
ω_c	$2eI_cR/\hbar$
ω_J	$\omega_{J0}\cos^{1/2}(\phi_0)$
ω_{J0}	plasma frequency $(2eI_c/\hbar C)^{1/2}$

a	antenna thickness, bridge radius
C	junction capacitance
c	velocity of light
d	wire distance in gauze (mesh)
e	electron charge
h	Planck's constant
$\hbar$	$h/2\pi$
$\bar{I}$	current bias
I_c	critical current
I_{c0}	current bias at zero response
k	Boltzmann's constant
L	junction inductance
l	antenna length
n	integer
R	junction resistance
R_H	resistance at maximum response (Fig. 7)
R_L	transition resistance (Fig. 7)
r	contact radius
T	absolute temperature
T^*	effect noise temperature
t	electrode distance
$\bar{V}$	average junction voltage
$\bar{V}_n$	average noise voltage
x	$\bar{I}/I_c$
Z_k	characteristic antenna impedance

ACKNOWLEDGMENTS

The author is grateful to C. D. Andriesse for his encouragement and criticism and to H. H. A. Schaeffer for his technical assistance.

[1]S. Ramo, J.R. Whinnery, and Th. van Duzer, *Fields and Waves in Communication Electronics* (Wiley, New York, 1965).
[2]K.K. Likharev and V.K. Semenov, Radio Eng. Electron. Phys. (USSR) **18**, 1734 (1973).
[3]H. Tolner, C.D. Andriesse, and H.H.A. Schaeffer, Infrared Phys. **16**, 213 (1976).
[4]C.C. Grimes, P.L. Richards, and S. Shapiro, J. Appl. Phys. **39**, 3905 (1968).
[5]D.E. McCumber, J. Appl. Phys. 39, 3113 (1968); W.C. Stewart, Appl. Phys. Lett. **12**, 277 (1968).
[6]J.E. Zimmerman, Proc. Appl. Superconductivity Conf., Annapolis, 1972, p. 544 (unpublished).
[7]J. Kurkijärvi and V. Ambegaokar, Phys. Lett. A **31**, 314 (1970).
[8]L.M. Matarrese and K.M. Evenson, Appl. Phys. Lett. **17**, 8 (1970).
[9]B. Twu and S.E. Schwarz, Appl. Phys. Lett. **26**, 672 (1975).
[10]J.D. Kraus, *Antennas* (McGraw-Hill, New York, 1950).
[11]H. Jasik, *Antenna Engineering Handbook* (McGraw-Hill, New York, 1961).
[12]J.J. Wijnbergen, W.H. Moolenaar, and G. de Groot, *Infrared Detection Techniques for Space Research* (Reidel, Dordrecht, 1972), p. 243.
[13]D.E. Prober, Rev. Sci. Instrum. **45**, 849 (1974).
[14]K.K. Likharev and L.A. Yakobson, IEEE Trans. Magn. **MAG-11**, 860 (1975).
[15]H. Kanter and F.L. Vernon Jr., Phys. Lett. A **32**, 155 (1970).
[16]B.T. Ulrich and E.O. Kluth, Proc. IEEE **61**, 51 (1973).
[17]G.A. Vanasse, A.T. Stair, Jr., and D.J. Baker, Aspen International Conference on Fourier Spectroscopy, 1970 (unpublished) [AFCRL-71-0019, 1971, Report No. 114 (unpublished)].
[18]H. Kanter and F.L. Vernon Jr., J. Appl. Phys. **43**, 3174 (1972).
[19]A.N. Vystavkin, V.N. Gubankov, L.S. Kuzmin, K.K. Likharev, V.V. Migulin, and V.K. Semenov, Rev. Phys. Appl. **9**, 79 (1974).
[20]A.N. Vystavkin, V.N. Gubankov, G.F. Leschenko, K.K. Likharev, and V.V. Migulin, Radio Eng. Electron. Phys. (USSR) **15**, 2121 (1970).
[21]V. Ambegaokar and A. Baratoff, Phys. Rev. Lett. **10**, 486 (1963).
[22]J. Baukus and J. Ballantyne, in Ref. 17, p. 415.
[23]F. Bedard and H. Meissner, Phys. Rev. **101**, 26 (1956).
[24]P.W. Anderson, *Progress in Low Temperature Physics VI*, edited by C.J. Gorter (North-Holland, Amsterdam, 1967), p. 1.
[25]S. Chandrasekhar, Rev. Mod. Phys. **15**, 1 (1943), Eq. 507.
[26]V. Ambegaokar and B.J. Halperin, Phys. Rev. Lett. **22**, 1364 (1969).
[27]T.A. Fulton, IEEE Trans. Magn. **MAG-11**, 749 (1975).
[28]T.A. Fulton, Phys. Rev. B **2**, 4694 (1970).
[29]N.F. Pedersen, J. Appl. Phys. **47**, 696 (1976).